ECS Transactions, 28 (3) 15-31 (2010)
10.1149/1.3367208 ©The Electrochemical Society

Synthesis and Characterization of Group IV Nanocrystals

L. Nikolova[a], D. Riabinina[b], B. Kadari[a], J.M. MacLeod[a,c], M. Chaker[a], F. Rosei[a,*]

[a] Institut National de la Recherche Scientifique, Center: Énergie, Matériaux et Télécommunications, Université du Québec, Varennes, Québec J3X 1S2, Canada
[b] Département de physique, Université de Montréal, Montréal, Québec H3C 3J7, Canada
[c] Dipartimento di Fisica, Università degli Studi di Trieste, Trieste 34127, Italy

[*]To whom correspondence should be addressed. Email: rosei@emt.inrs.ca

Abstract

The first reports that nanostructured silicon emits radiation in the visible wavelength date back twenty years. This observation is interesting from a fundamental point of view and is potentially important for device engineering, as it points to the opportunity of combining microelectronics and optoelectronics on the same silicon chip. This combination is becoming increasingly attractive due to the intrinsic limitations that are being met by the microelectronics industry in its attempt to progressively reduce device features. In this review, we describe and compare the structure and properties of group IV nanocrystals (mostly silicon, with some references to germanium) grown by ion implantation and reactive pulsed laser deposition. Particular emphasis is placed on structural and spectroscopic characterization, as well as size-dependent optical properties. The origin of the luminescence signal and the role of defects and interfaces are discussed in detail.

Introduction

Miniaturization of features in microelectronic devices has proceeded exponentially for several decades (1), yet is expected to soon be limited by technological challenges as well as intrinsic physical limitations. A possible solution to such problems is to replace electrical signals with photons transported through optical interconnections.

Most conventional microelectronics devices are based on group IV semiconductors, in particular, silicon and silicon-germanium strained films. However, silicon and germanium are not well-suited for optoelectronic applications due to their indirect band gap and consequent limited luminescence efficiency. For example, light emission in bulk silicon requires photon-phonon coupling to satisfy momentum conservation, and the probability for this process is very low. Generally, if an exciton is generated, the de-excitation takes place on non-radiative centers, such as defects in the crystal structure.

Quantum confinement effects may arise in nanoscale systems, and may be exploited to harness specific functionalities and properties that are absent in the bulk material (2). For example, nanostructured silicon is a luminescent material and a potential light emission

Downloaded 13 Sep 2010 to 137.122.27.231. Redistribution subject to ECS license or copyright; see http://www.ecsdl.org/terms_use.jsp

source (3). This introduces the possibility to obtain integrated optoelectronic circuits entirely based on silicon, a prospect which has led to increasing research efforts over the last two decades. Particular research attention has been focused on two forms of nanostructured silicon that emit in the visible range: porous silicon and silicon nanocrystals (Si-nc) embedded in a silicon dioxide matrix (SiO_2) (4, 5). The latter configuration is more suitable for applications since the system is chemically stable, rigid and the emitted wavelength can be controlled by controlling the size of the nc. Alloying silicon with germanium introduces the possibility for light emission from other types of nanostructures (6-8).

Group IV nanocrystals and porous films can be synthesized using different techniques such as sputtering, ion implantation (9), plasma enhanced chemical deposition (PECVD) (10, 11) and reactive pulsed laser deposition (RPLD) (12-19). These systems have been intensely investigated both from the theoretical (20-23) and experimental (24-26) points of view, focusing in particular on their growth, structural characterization and luminescence properties (where applicable), with a view to understanding the relation between their structure and their optical properties.

In this review, we discuss two methods for the synthesis of group IV nc: ion implantation and pulsed laser deposition (PLD), with particular attention to the experimental parameters that can be tuned to control the emission properties of the resulting nc. PLD can also be used for the synthesis of porous films (12). We will focus in particular on silicon, even though most synthesis and structural concepts can be applied to germanium as well. We also show that their photoluminescence (PL) spectra depend on a combination of effects, and we present a brief overview of strategies for increasing PL efficiency. Finally, we present a model that describes the spatial distribution of PLD-formed Si-nc within the oxide matrix.

Synthesis methods for Group IV nc: advantages and disadvantages

The principle of formation of silicon and germanium nc in oxide matrices is the same for any of the experimental techniques used to synthesize them. In the case of silicon, a layer of silicon-rich silicon oxide is grown on a substrate, generally a silicon wafer, either through the deposition of a thin film or implantation of extra silicon species into a thermally-grown oxide layer. The second step consists of a high-temperature (~1100°C) annealing of the silicon sub-stoichiometric oxide, to promote atomic diffusion in the sample followed by the crystallization of nanometer sized silicon crystallites. Depending on their structural properties, these Si-nc may exhibit luminescence properties. The exact properties of the final Si-nc depend on their structural features and the chemical composition of the silicon substoichiometric oxide, together with the annealing parameters.

Ion implantation is the most widely-used technique for the synthesis of Si-nc. Its advantage lies in the possibility to control the properties of the nc via the energy and the fluence of implantation. The energy determines the profile and the depth of the implanted silicon ions, while the fluence provides control over the Si-nc sizes (27). Furthermore, ion implantation is already used in the microelectronics industry, so the integration of ion-implanted optoelectronic components with current architectures could be possible at a relatively low fabrication cost.

RPLD (13) is an emerging technique which consists in depositing a layer of silicon-rich oxide by laser ablation of silicon under a low oxygen pressure, followed by annealing.

Downloaded 13 Sep 2010 to 137.122.27.231. Redistribution subject to ECS license or copyright; see http://www.ecsdl.org/terms_use.jsp

The main advantage of RPLD versus ion implantation is in the uniformity of the depth profile of the substoichiometric oxide layer, which creates the possibility to produce nanocrystal-containing films of arbitrary thickness. On the other hand, the lateral distribution in PLD can be quite non-uniform. In conventional PLD with a fixed substrate, the thickness of the deposited layer remains constant only over areas as small as 1 cm^2. However, new commercial systems offer large-scale scanning of substrates during the deposition process, allowing the growth of thin films with reasonable thickness uniformity on areas as large as 10 cm in diameter. The possibility for the synthesis of Si-nc films using this equipment makes pulsed laser ablation extremely interesting for fundamental research as well as for potential industrial applications.

Photoluminescence from Si-nc: Overview

Numerous articles in the literature describe the interpretation of the luminescence spectra of Si-nc systems. A large number of studies have been performed on the influence of size and distribution (13, 28, 29), of temperature (30, 31), of annealing parameters (32), as well as specific parameters of the synthesis methods (33, 34). However, the physical mechanisms of carrier recombination in such nanostructures are still poorly understood.

Quantum confinement leads to a relationship between the size and the electronic structure of Si-nc and defines the possibility of tuning the emission wavelength by tuning nanocrystal size. Many descriptions of quantum confinement have been offered, including fairly elaborate models based on first principles calculations (13, 35-39) and density functional theory (DFT) calculations (40). All these models predict a blue shift in the bandgap structure of silicon nanostructures with increased confinement, in agreement with experimental data.

Another mechanism salient to carrier recombination in Si-nc is spatial confinement (14, 33, 41). The latter decreases the probability of recombination of carriers on non-radiative sites and is not related to the electronic structure of silicon. The observed emission is thus not dependent on the size of the nanoparticles involved. Additionally, interface states between the Si-nc and the surrounding oxide matrix may provide additional PL peaks whose position is not dependent on Si-nc size (30, 42, 43).

Since the PL properties of Si-nc depend critically on their structure, controlling the nanocrystal size and quality via careful control of the synthesis parameters is crucial. In the following sections we provide an overview of the relationship between experimental parameters, structure and PL for Si-nc synthesized by RPLD and ion implantation. The systems that we describe here are case studies, and provide an indication of just how much control can be exerted over the Si-nc growth process. Obviously the parameter space for tuning the experimental parameters is extremely wide, and the exact experimental implementation depends on the properties required of the Si-nc.

Downloaded 13 Sep 2010 to 137.122.27.231. Redistribution subject to ECS license or copyright; see http://www.ecsdl.org/terms_use.jsp

Controlling the Structure and PL of Si-nc via Synthesis Parameters: RPLD

Synthesizing Si-nc by RPLD

In RPLD, the synthesis of Si-nc requires the deposition of silicon-rich silicon dioxide films (SiO_x, $0 < x < 2$). Subsequently, high-temperature annealing (> 1000 °C for one hour) under an inert atmosphere precipitates the excess silicon in the oxide film, forming Si-nc in the SiO_2 matrix. The Si-nc size is directly controlled by the excess silicon quantity in the Si-rich oxide films: higher excess leads to a larger Si-nc size. Therefore, the key issue in the synthesis of Si-nc embedded in a SiO_2 matrix is the control of the excess Si.

The composition of the silicon oxide films can be precisely controlled by varying the background oxygen pressure during the ablation process. The degree of oxidation of as-deposited SiO_x films progressively increases with increasing background oxygen pressure, as shown by the x-ray photoelectron spectroscopy (XPS) measurements reported in Figure 1 (16). At low O_2 pressure (0.03 mTorr), the Si 2p spectrum indicates that the film mainly consists of nonoxidized Si (Si^0 peak at 99.3 eV). Spectral contributions at higher binding energy, resulting from silicon oxidation, gradually appear with increasing oxygen pressure. At the highest oxygen pressure used (1.5 mTorr), the films are found to be mainly composed of SiO_2 (Si^{4+} peak at 103.3 eV).

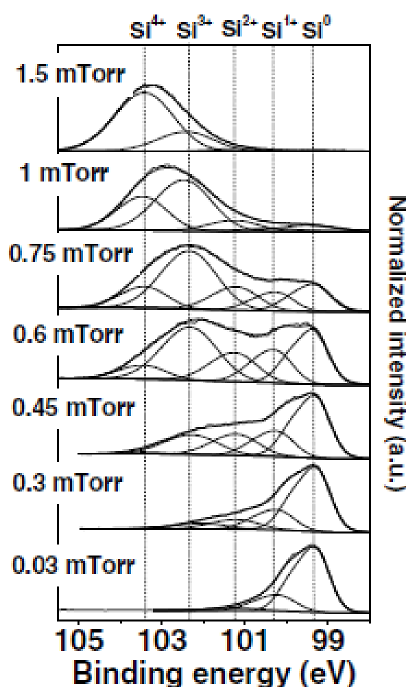

Figure 1 Si 2*p* XPS spectra of as-deposited films for oxygen pressures varied from 0.03 to 1.5 mTorr. All spectra were fitted with five peaks corresponding to silicon (Si^0), suboxide (Si^{1+}, Si^{2+}, and Si^{3+}), and SiO_2 (Si^{4+}) contributions (16).

The average size of the Si-nc was estimated from XRD peak width using a standard Scherrer analysis (44,45). Figure 1a shows the evolution of the Si(111) XRD peak as a function of background oxygen pressure, and Figure 1b shows that the corresponding Si-

Downloaded 13 Sep 2010 to 137.122.27.231. Redistribution subject to ECS license or copyright; see http://www.ecsdl.org/terms_use.jsp

nc size decreases with increasing oxygen pressure. This demonstrates that by tuning the background oxygen pressure during deposition, RPLD can be used to control Si-nc size.

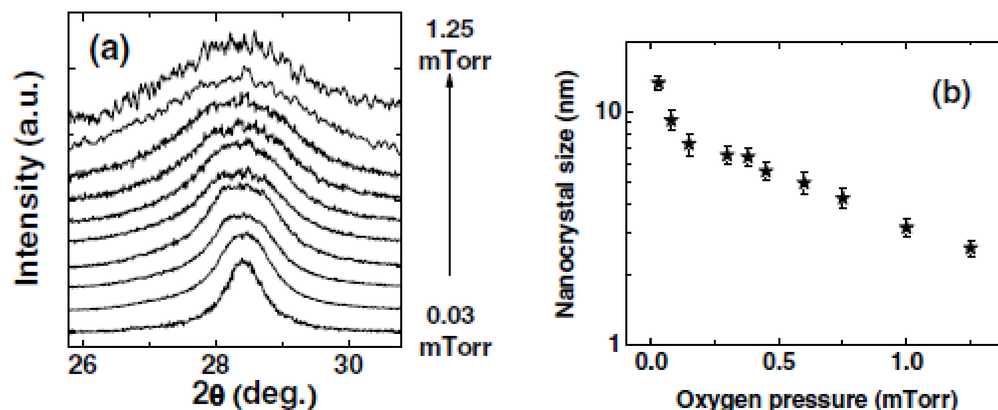

Figure 2 (a) Normalized (111) XRD spectra of Si-nc as a function of oxygen pressure varied from 0.03 to 1.25 mTorr (16). (b) Evolution of Si-nc size as function of oxygen pressure (17). The error bars for were determined by full width at half-maximum measurements from the (111) reflection.

Cross-sectional high resolution transmission electron microscopy (HRTEM) measurements of annealed samples were performed to observe individual Si–nc in the oxide matrix. Figure 3 shows typical HRTEM images and corresponding size distribution histograms for annealed samples deposited at 1 and 0.15 mTorr O_2, respectively. The average nc size is found to be 5.6 ±1.0 nm for 0.15 mTorr and 2.6±0.5 nm for 1 mTorr. The size distribution of Si-nc embedded in an oxide matrix is narrow, compared to nanoparticles obtained by PLD in an inert gas.

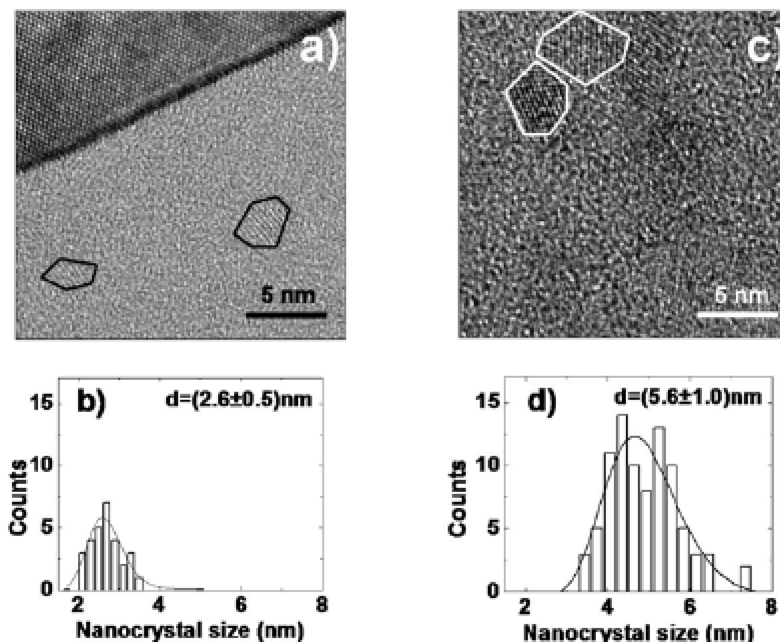

Figure 3 Si-nc HRTEM images and size histograms are shown for 3.3% (a, b) and 52% (c, d) Si^0 volume fraction samples (16).

Downloaded 13 Sep 2010 to 137.122.27.231. Redistribution subject to ECS license or copyright; see http://www.ecsdl.org/terms_use.jsp

PL of RPLD-synthesized Si-nc

For RPLD-synthesized Si-nc, PL has been observed for samples containing Si–nc with sizes varying from 1.9 to 6.4 nm (17, 33). Figure 4 shows typical PL spectra of Si-nc in SiO_2 as a function of their size (17). The PL intensity increases with decreasing nc size and reaches its maximum at 2.6 nm. This behaviour is in agreement with the expected quantum confinement effect in indirect gap semiconductors characterized by an increasing intensity with decreasing nc size. For sizes below 2.6 nm, the intensity decrease can be attributed to the low volume density of nanocrystals and/or low absorbance of the sample with composition close to silicon oxide. The position of the PL spectral maximum shifts from 740 nm (1.67 eV) to 920 nm (1.35 eV) with an increase in nanocrystal size from 1.9 nm to 6.4 nm. The possibility of controlling the PL peak position by varying nanocrystal size is highly promising for future optoelectronic silicon-based applications.

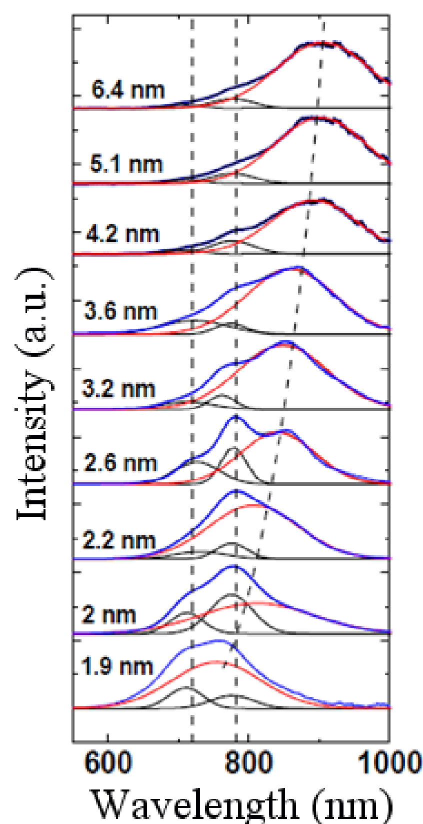

Figure 4 PL spectra as a fucntion of Si-nc size.

Deconvolution of the peaks in Figure 4 provides insight into the mechanisms contributing to the PL. Three peaks can be distinguished in each spectrum: two peaks that arise at fixed positions (720 and 780 nm), and one peak whose position varies as a function of Si-nc size. Based on the works of Degoli et al. (42) and Kanemitsu et al. (43), the peak at 720 nm can be attributed to the lack of oxygen at the Si-nc/SiO_2 interface while the peak at 780 nm can be attributed to interface states. The variation of the position of the third peak as a function of nanocrystal size suggests that it originates from quantum confinement.

Downloaded 13 Sep 2010 to 137.122.27.231. Redistribution subject to ECS license or copyright; see http://www.ecsdl.org/terms_use.jsp

Table I shows the evolution of the position of three peaks obtained from the deconvolution of the PL spectra as a function of Si-nc size. The peak E_1 (associated with quantum confinement) shifts from 750 to 900 nm as the Si-nc size increases from 1.9 to 6.4 nm. For nc larger than 4.2 nm, the peak shift is negligible but its intensity decreases by a factor of five. It is possible that for nc sizes over 4.2 nm, spatial confinement effects dominate over quantum confinement.

Table I The position of the three contributions to the PL spectra shown in **Figure 4** as a function of Si-nc size.

Si-nc size (nm)	E_1 (nm)	E_2 (nm)	E_3 (nm)
1.9 (± 0.2)	753 (± 8)	777 (± 8)	711 (± 8)
2.0 (± 0.3)	811 (± 8)	775 (± 8)	712 (± 8)
2.2 (± 0.3)	807 (± 8)	775 (± 8)	731 (± 8)
2.6 (± 0.4)	840 (± 8)	778 (± 8)	727 (± 8)
3.2 (± 0.4)	848 (± 8)	762 (± 8)	713 (± 8)
3.6 (± 0.6)	859 (± 8)	774 (± 8)	722 (± 8)
4.2 (± 0.6)	893 (± 8)	769 (± 8)	722 (± 8)
5.1 (± 0.6)	901 (± 8)	774 (± 8)	722 (± 8)
6.4 (± 0.6)	907 (± 8)	774 (± 8)	722 (± 8)

The shift of the quantum confinement related peak has been compared to the experimental and theoretical results reported in the literature (Figure 5). The results obtained for the PL spectra of Si-nc synthesized by RPLD are in agreement with the reported experimental results. However, the experimental data do not perfectly match the theoretical predictions (dashed line), in particular for the smallest nanocrystals. This discrepancy is often explained by exciton effects in quantum dots. Indeed, the interaction between several highly confined charge carriers may induce multi-excitonic states with the energy below the DFT-calculated band energy (37).

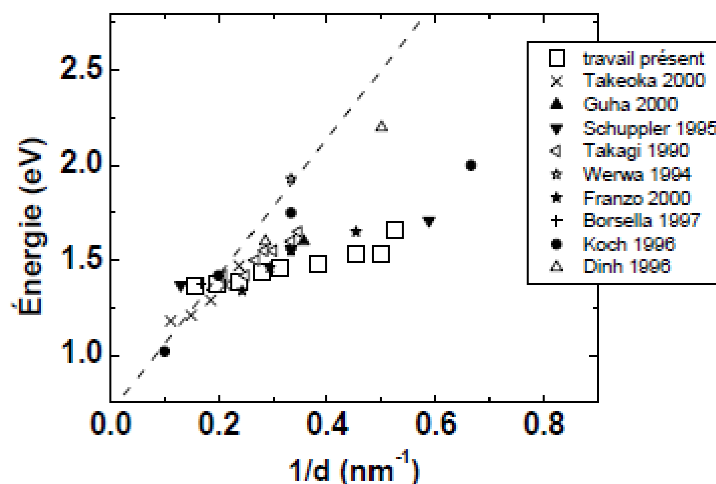

Figure 5 The position of PL peak as a function of parameter 1/d (where d is the nc size) for Si-nc in various systems (Refs. (4, 46-53)) Dashed line represents theoretical results from Ref. (40).

Downloaded 13 Sep 2010 to 137.122.27.231. Redistribution subject to ECS license or copyright; see http://www.ecsdl.org/terms_use.jsp

Controlling the Structure and PL of Si-nc via Synthesis Paramters: Ion Implantation

Synthesizing Si-nc via Ion Implantation

The formation of_Si-nc by ion implantation can concurrently lead to the formation of substoichiometric oxides due to damage inflicted by the Si+ ions entering the SiO_2/Si target. It has been found that substoichimeric oxides of SiO_1 (Si^{+1}) and SiO_2 (Si^{+2}) form at very low concentrations as compared to the SiO_3 (Si^{+3}) and SiO_4 (Si^{+4}) suboxides (54). At low fluences SiO_3 is comparable in concentration to the stoichiometric silicon dioxide at the implantation range, while at high fluences the substoichiometric oxide concentrations are very low. The same results have been obtained for higher energy of implantation at equivalent fluence (51).

TEM studies have found that the distribution of Si-nc follows the profile of implantation; the largest Si-nc are found in the densely-populated center of the profile, and the smallest Si-nc are dispersed in the lower-nc-density periphery. The minimal size for the nc has been found to be 1.8 nm, with an uncertainty of a half atomic plane (0.3 nm). At high fluences, Si-nc sizes vary significantly and the crystals can be as large as 20 nm in size (Figure 6). In addition, discrete stable size regimes can be identified. For the fluence shown in Figure 6a, three distributions with mean sizes of ~4 nm, ~9 nm and ~12 nm are visible. However, overall, the mean particle size is energy and fluence dependant (55). With decreasing fluence, the size distribution becomes unimodal (Figure 6b) and finally becomes unimodal and quite narrow at low fluences (Figure 6c) (For the lowest fluence where the contrast in the images was poor annular dark field scanning TEM (ADF STEM) measurements were performed to obtain a better statistics for the size distribution. HRTEM measurements have been made on the same sample and the two techniques have shown the same distribution in sizes (54)).

An examination of the Si-nc structure within a sample formed at an intermediate fluence (1×10^{17} Si^{+}/cm^{2} at 50 keV) has shown that an amorphous phase is present after annealing (56). This result, obtained with dark field TEM (DF TEM), ADF STEM and Z contrast TEM, is consistent with results obtained by Raman spectroscopy (56).

Downloaded 13 Sep 2010 to 137.122.27.231. Redistribution subject to ECS license or copyright; see http://www.ecsdl.org/terms_use.jsp

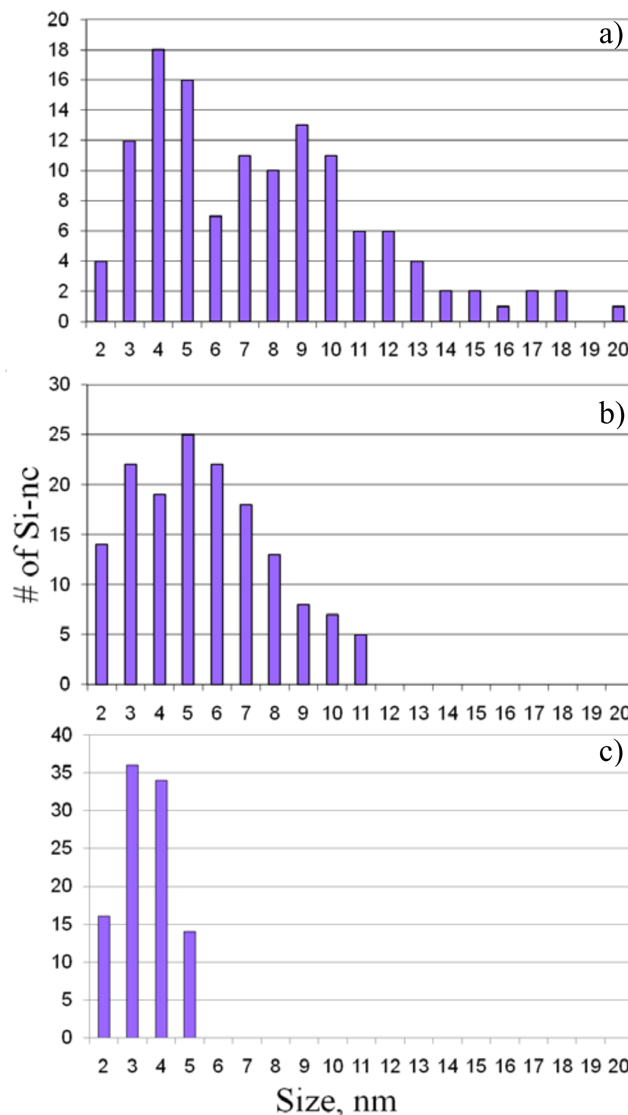

Figure 6 Size distribution of Si-nc for ion implantation fluences of a) 1.9×10^{17} Si^{+}/cm^{2}, b) 1.0×10^{17} Si^{+}/cm^{2} and c) 7.0×10^{16} Si^{+}/cm^{2}, at 50 keV. Measurements were obtained via dark field TEM (a and b) and by ADF STEM imaging (c).

PL of ion implantation-synthesized Si-nc

For Si-nc obtained via ion implantation in a SiO_2 matrix, the PL spectrum is strongly dependant on the ion fluence, which determines the percentage of excess silicon and the size of the Si-nc. Figure 7 shows the PL spectra of typical Si-nc in a 152 nm thick SiO_2 layer for different fluences of implantation ranging from 3×10^{16} Si^{+}/cm^{2} to 19×10^{16} Si^{+}/cm^{2}. The shift in mean emission wavelength with fluence follows the trend exhibited by the measured size: lower fluence favors the formation of smaller particles, which correlates with shorter wavelength emission. At lower fluences, the PL spectra probably also reflect the substroichiometric oxides adding states in the Si band gap and resulting in a broader PL spectrum.

Downloaded 13 Sep 2010 to 137.122.27.231. Redistribution subject to ECS license or copyright; see http://www.ecsdl.org/terms_use.jsp

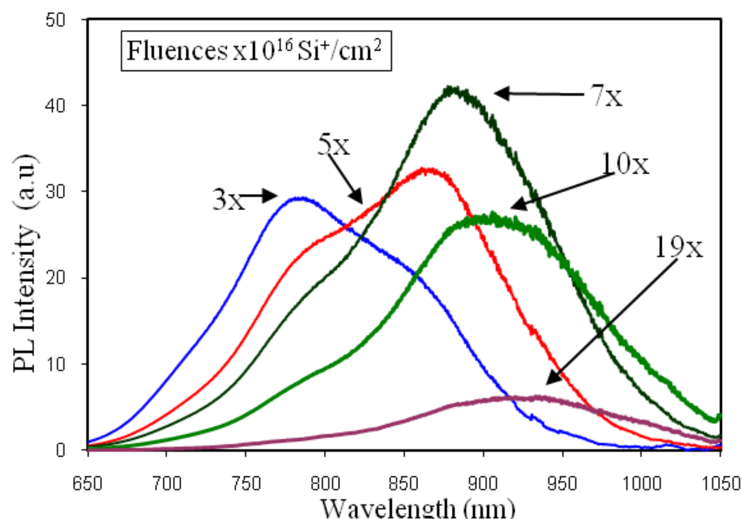

Figure 7 PL spectra for Si-nc obtained by ion implantation at 50 keV. The fluences are given in the legend with units of $\times 10^{16}$ Si/cm^2.

HRTEM further reveals that the nc up to 5 nm in diameter are free of defects and exhibit a circular shape, while larger particles are generally elongated and contain defects (57). It is believed that these defects are responsible for decreasing the PL intensity and are centers for nonradiative de-excitation. Maximal PL intensity in the visible spectrum has been found for crystals around 3 nm in size and it is now accepted that the larger, defect-free crystals contribute to the near IR spectrum (57).

Electroluminescence of Si-nc obtained by ion implantation

Some preliminary investigations into the electroluminescence (EL) of Si-nc have been performed. These studies are crucial for the development of specific devices, for example, light-emitting diodes. The best results have been obtained on p-type silicon (100) wafers (1-10 Ω.cm, 270 μm thick) with 37 nm of SiO_2. The native oxide layer on the back side of the wafer was removed by HF etching. A silver contact was fabricated on the oxide-free back side, while a semitransparent gold contact was deposited of the front side. Si-nc were formed via a two-stage ion implantation procedure: 2.5×10^{16} Si^+/cm^2 at 25 keV followed by 1.0×10^{16} Si^+/cm^2 at 12 keV. This approach has the benefit of forming an almost-uniform Si-nc band through the entire thickness of SiO_2. In addition, the roughness introduced by the implantation at 25 keV may increase the probability for charge carriers to tunnel through the SiO_2 film to reach the silicon substrate.

EL measurements, shown in Figure 8, have been taken at a single luminescent spot. The same type of spot EL has also been observed by Valenta et al. (58). Three peaks are present. The first peak, at 647 nm, is attributed mainly to non-bringing oxygen hole center (NBOHC) defects in the oxide (59); the second and third peaks, at 804 nm and 879 nm, are attributed to the presence of the Si-nc, as the peaks positions coincide with the PL peak situated in the range ~ 750–950 nm, and for these peaks the intensity increases with the applied voltage. In samples without Si-nc, no peaks with these positions have been observed. More details can been found in Ref. (60).

Downloaded 13 Sep 2010 to 137.122.27.231. Redistribution subject to ECS license or copyright; see http://www.ecsdl.org/terms_use.jsp

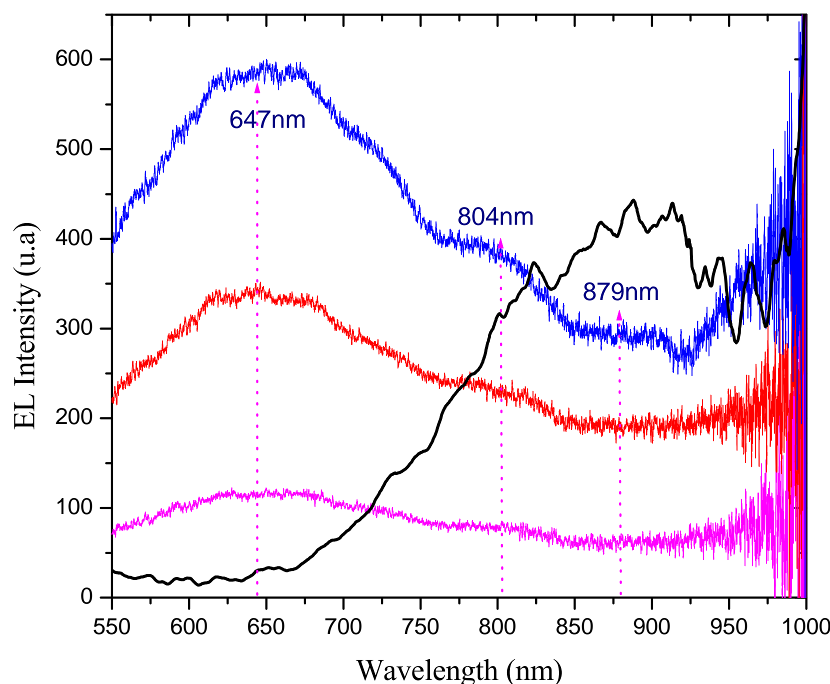

Figure 8 Micro-EL and PL spectra for Si-nc (60).

Methods for improving PL Efficiency

In the Si/SiO_2 system, there exist various mechanisms for the non-radiative recombination of charge carriers generated by the excitation source. Dangling-bond defects at the Si-nc/SiO_2 interface are known to contribute strongly to the quenching of PL. The most widely-used method for reducing non-radiative recombination due to the interface defects is hydrogen passivation. During this annealing procedure (at 500 °C under partial hydrogen and nitrogen pressure in 5/95 proportion), hydrogen molecules diffuse into the material and saturate dangling bonds (61-63). The overall efficiency of the method depends on passivation time, temperature and hydrogen pressure (53, 62), as well as the initial quality of the Si-nc.

Finally, we note that Er- or other rare earth-doped Si-nc exhibit remarkable PL properties. In these systems, Si-nc capture charge carriers and transfer the energy to the dopant atoms. The radiative recombination observed in the PL spectrum corresponds to the atomic transitions in the dopant. Thus, this system aims to improve erbium luminescence using the quantum confinement in Si-nc (64, 65).

Downloaded 13 Sep 2010 to 137.122.27.231. Redistribution subject to ECS license or copyright; see http://www.ecsdl.org/terms_use.jsp

Nucleation, Growth, and Spatial Distribution of RPLD-Syntheized Si-nc

HRTEM, XPS and XRD characterization clearly demonstrate that the Si-nc size is directly controlled by the quantity of excess silicon in the Si-rich oxide films. The oxygen pressure in RPLD determines the Si^0 volume fraction, $f_{Si0,}$ in the Si/SiO_2 system as well as the Si-nc size, d_{XRD}. To understand the formation process of Si-nc, a correlation between the non-oxidized Si volume fraction, f_{Si0}, and the Si-nc size previously measured by XRD, d_{XRD}, was investigated (16). This correlation between f_{Si0} and d_{XRD} is based on the following assumptions:

(a) The non-oxidized Si concentration CSi^0 remains constant after annealing (66).

(b) Amorphous Si agglomerates and/or very small nanocrystals (not observed by XRD due to their amorphous nature or low concentration but detected by XPS) are not present in the sample, as confirmed by Raman spectroscopy and HRTEM images (16).

(c) The nanocrystal size estimated by XRD is reduced by 0.4 nm, which corresponds to the thickness of the sub-oxide shell (66, 67), not detected in the Si^0 peak in XPS measurements.

Figure 9 shows the correlation between nc core size (obtained from XRD and HRTEM measurements) as a function of non-oxidized Si volume fraction (measured by XPS), recently reported by Riabinina and co-workers (16). Riabinina et al. proposed a simple model for the distribution of nanocrystals in a Si oxide matrix, grown by laser ablation (applying the model to other synthesis approaches is possible yet not straightforward, since it assumes that there is no residual amorphous silicon dioxide in the matrix, which occurs for example in the case of ion implantation). According to this model, the nanocrystals are assumed to be arranged in a simple cubic lattice configuration with typical distance L between the centers of nanoparticles, as schematically shown in Figure 10.

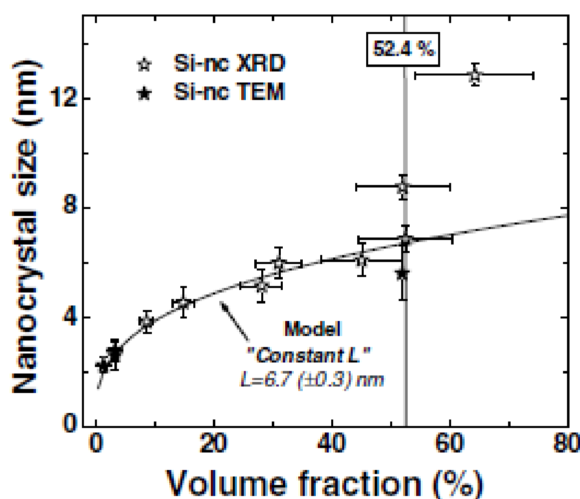

Figure 9 Nanocrystal core size extracted from XRD and HRTEM data versus Si^0 volume fraction obtained by XPS (16).

Downloaded 13 Sep 2010 to 137.122.27.231. Redistribution subject to ECS license or copyright; see http://www.ecsdl.org/terms_use.jsp

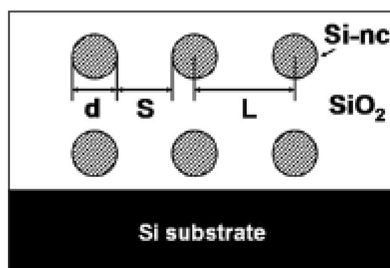

Figure 10 Scheme of simple cubic lattice distribution model of Si nanocrystals in a Si oxide matrix (16).

From this simple distribution model, the Si^0 volume fraction f_{Si0} may be directly related to the nanocrystal core size d_{core} by:

$$\frac{f_{Si^0}}{100} = \frac{\frac{3}{4}\pi\left(\frac{d_{core}}{2}\right)^3}{L^3} \qquad [1]$$

Assuming that the distance between the nanocrystal centers is constant, the data from Figure 9 were fitted using this model. In this case, the average size may be expressed as follows:

$$d_{core} = L\,(6f_{Si}{}^{0} / 100\,\pi)^{1/3} \qquad [2]$$

The best fit is obtained when the distance L between nanocrystal centers is equal to (6.7 ± 0.3) nm. Additional measurements demonstrated that the nanocrystal size stabilizes for annealing temperatures and times over 1050 °C and 1 h, respectively.

According to nucleation and growth theory, energetic factors will drive some nanocrystals to grow, drawing mass from others, which shrink (Ostwald ripening). When their size reaches the critical size d^*, the nanocrystals tend to grow, thus reducing the energy of the system. When such nanocrystals are formed, their center positions remain fixed. Therefore, the *"constant L"* model, described previously, can be attributed to the nucleation regime in which the nuclei centers are in stable positions. For $f_{Si0} > 50\%$, the simple cubic lattice configuration model is not valid. In fact, the volume fraction corresponding to the situation in which the nanocrystals are in contact (i.e. $S = 0$) is equal to 52.4%. Therefore, the increase by a factor of two of Si nanocrystal size for $f_{Si0} > 50\%$ could be explained by the coalescence of two or more nanocrystals.

Conclusions and Perspectives

In this short review, we have discussed the growth and characterization of group IV nanocrystals in an oxide matrix, mostly drawing examples from work performed at INRS. We largely focused on the case of Si-nc, which is potentially more interesting for industrial applications. In particular we described synthesis approaches based on ion implantation (so far the most widely used technique) and RPLD, with comparisons and ample discussions on the structural and optical properties of the resulting nanocrystals. An important challenge

Downloaded 13 Sep 2010 to 137.122.27.231. Redistribution subject to ECS license or copyright; see http://www.ecsdl.org/terms_use.jsp

that remains to be addressed is the relative effect of defects and interfaces on the overall luminescence properties. In particular, it has been shown that hydrogen can passivate defects such as dangling bonds, leading to higher luminescence signals.

We note that EL results, which are extremely important for the development of Si-based lasers, are still few and far between, largely due to the challenge of making an electrical current flow through an oxide matrix, which is obviously insulating. An interesting perspective is to grow the nanocrystals directly in a conductive matrix, such as e.g. silicon nitride or a conductive organic thin film.

Another important challenge towards the goal of controlling structure/property relations in nanostructured materials is to image their nucleation as it occurs, i.e. with a high time resolution. Recently developed dynamic transmission electron microscopes have demonstrated a time resolution of about 10 ns while maintaining a spatial resolution of about 10 nm (68-73). While these lateral and temporal resolutions are insufficient to make a full movie of nanocrystal nucleation, second generation DTEMs are likely to bring us closer to that objective.

The integration of optoelectronic components with microelectronics architectures will require precise control over their placement. In the case of PLD-deposited structures, we have recently demonstrated that stencils with nanoscale features (74-77) can be used to pattern germanium features on the scale of hundreds of nanometers (78). Although this length scale is obviously too large for the controlled fabrication of single Si-nc, it presents an opportunity for systematically positioning PL-active regions of Si-nc in an oxide matrix.

Finally, strain is known to affect the electronic and optical properties of thin films and nanostructures, however measuring strain with nanometer scale lateral resolution is currently not possible. It has been recently shown that x-ray photoemission electron microscopy can be used to obtain chemical maps of Ge/Si nanostructures (79-82). It should be possible to extend the use of this technique to measure strain (67) with sub 100 nm lateral resolution, with implications for the growth of group IV nanocrystals and their use in devices.

Acknowledgements

F.R. and M.C. are grateful to the Canada Research Chairs program for partial salary support. L.N., D.R., J.M.M. acknowledge NSERC for post-graduate (L.N.) and post-doctoral (D.R. and J.M.M.) fellowships. F.R. and M.C. are grateful to NSERC for support through NSERC Discovery and Strategic grants.

References

1. G.E. Moore, *Electronics*, **38**, 114 (1965).
2. F. Rosei, *J. Phys. - Cond. Mat.*, **16**, S1373 (2004).
3. Z. Yuan, A. Anopchenko, N. Daldosso, R. Guider, D. Navarro-Urrios, A. Pitanti, R. Spano, and L. Pavesi, *Proc. IEEE*, **97**, 1250 (2009).
4. H. Takagi, H. Ogawa, Y. Yamazaki, A. Ishizaki, and T. Nakagiri, *Appl. Phys. Lett.*, **56**, 2379 (1990).

Downloaded 13 Sep 2010 to 137.122.27.231. Redistribution subject to ECS license or copyright; see http://www.ecsdl.org/terms_use.jsp

5. L.T. Canham, *Appl. Phys. Lett.*, **57**, 1046 (1990).
6. R. Apetz, L. Vescan, A. Hartmann, C. Dieker, and H. Luth, *Appl. Phys. Lett.*, **66**, 445 (1995).
7. J. Brunner, T.S. Rupp, H. Gossner, R. Ritter, I. Eisele, and G. Abstreiter, *Appl. Phys. Lett.*, **64**, 994 (1994).
8. K. Brunner, *Rep. Prog. Phys.*, **65**, 27 (2002).
9. G.G. Ross, D. Barba, C. Dahmoune, Y.Q. Wang, and F. Martin, *Nucl. Instrum. Methods Phys. Res., Sect. B*, **256**, 211 (2007).
10. G.V. Prakash, N. Daldossa, E. Degoli, F. Iacona, M. Cazzanelli, Z. Gaburro, G. Pucker, P. Dalba, F. Rocca, E.C. Moreira, G. Franzo, D. Pacifici, F. Priolo, C. Arcangeli, A.B. Filonov, S. Ossicini, and L. Pavesi, *J. Nanosci. Nanotechnol.*, **1**, 159 (2001).
11. L. Dal Negro, M. Cazzanelli, N. Daldosso, Z. Gaburro, L. Pavesi, F. Priolo, D. Pacifici, G. Franzo, and F. Iacona, *Physica E*, **16**, 297 (2003).
12. D. Riabinina, M. Chaker, and F. Rosei, *Appl. Phys. Lett.*, **89**, 131501 (2006).
13. D. Riabinina, C. Durand, M. Chaker, and F. Rosei, *Appl. Phys. Lett.*, **88**, 073105 (2006).
14. J. Derr, K. Dunn, D. Riabinina, F. Martin, M. Chaker, and F. Rosei, *Physica E*, **41**, 668 (2009).
15. D. Riabinina, C. Durand, M. Chaker, N. Rowell, and F. Rosei, *Nanotechnology*, **17**, 2152 (2006).
16. D. Riabinina, C. Durand, J. Margot, M. Chaker, G.A. Botton, and F. Rosei, *Phys. Rev. B*, **74**, 075334 (2006).
17. D. Riabinina, C. Durand, F. Rosei, and M. Chaker, *Phys. Status Solidi A*, **204**, 1623 (2007).
18. D. Riabinina, F. Rosei, and M. Chaker, *J. Exp. Nanosci.*, **1**, 83 (2006).
19. K. Dunn, J. Derr, T. Johnston, M. Chaker, and F. Rosei, *Phys. Rev. B*, **80,** 9 (2009).
20. J. Carreras and B. Garrido. *2008 5th International Conference on Group IV Photonics, GFP*, **326**, art. no. 4638188 (2008).
21. J. Carreras, O. Jambois, M. Peralvarez, Y. Lebour, and B. Garrido, *Microelectron. Eng.*, **85**, 2378 (2008).
22. J. Valenta, A. Fucikova, I. Pelant, K. Kusova, K. Dohnalova, A. Aleknavicius, O. Cibulka, A. Fojtik, and G. Kada, *New J. Phys.*, **10**, art. no. 073022 (2008).
23. D. Flyura, B. Marie, and N. Kai, *Nucl. Instrum. Methods Phys. Res., Sect. B*, **266**, 2683 (2008).
24. M. Porti, M. Avidano, M. Nafria, X. Aymerich, J. Carreras, O. Jambois, and B. Garrido, *J. Appl. Phys.*, **101**, 056101 (2007).
25. J. Barreto, M. Peralvarez, J.A. Rodriguez, A. Morales, M. Riera, M. Lopez, B. Garrido, L. Lechuga, and C. Dominguez, *Physica E*, **38**, 193 (2007).
26. X.Y. Chen, Y.F. Lu, Y.H. Wu, B.J. Cho, L.J. Tang, D. Lu, and J.R. Dong, *Appl. Surf. Sci.*, **253**, 2718 (2006).
27. Y.Q. Wang, R. Smirani, and G.G. Ross, *Nanotechnology*, **15**, 1554 (2004).
28. T. Inokuma, Y. Wakayama, T. Muramoto, R. Aoki, Y. Kurata, and S. Hasegawa, *J. Appl. Phys.*, **83**, 2228 (1998).
29. F. Iacona, C. Bongiorno, C. Spinella, S. Boninelli, and F. Priolo, *J. Appl. Phys.*, **95**, 3723 (2004).
30. Y. Kanemitsu, T. Ogawa, K. Shiraishi, and K. Takeda, *Phys. Rev. B*, **48**, 4883 (1993).
31. X.X. Wang, J.G. Zhang, L. Ding, B.W. Cheng, W.K. Ge, J.Z. Yu, and Q.M. Wang, *Phys. Rev. B*, **72**, 195313 (2005).

Downloaded 13 Sep 2010 to 137.122.27.231. Redistribution subject to ECS license or copyright; see http://www.ecsdl.org/terms_use.jsp

32. T. Shimizu-Iwayama, N. Kurumado, D.E. Hole, and P.D. Townsend, *J. Appl. Phys.*, **83**, 6018 (1998).
33. D. Riabinina, C. Durand, M. Chaker, and F. Rosei, *COLA'05: 8th International Conference on Laser Ablation*, **59**, 189 (2007).
34. R. Smirani, F. Martin, G. Abel, Y.Q. Wang, and G.G. Ross, *Nanotechnology*, **16**, 32 (2005).
35. T. Takagahara and K. Takeda, *Phys. Rev. B*, **46**, 15578 (1992).
36. V. Ranjan, V.A. Singh, and G.C. John, *Phys. Rev. B*, **58**, 1158 (1998).
37. E. Dekel, D. Gershoni, E. Ehrenfreund, J.M. Garcia, and P.M. Petroff, *Phys. Rev. B*, **61**, 11009 (2000).
38. A.J. Read, R.J. Needs, K.J. Nash, L.T. Canham, P.D.J. Calcott, and A. Qteish, *Phys. Rev. Lett.*, **69**, 1232 (1992).
39. D. Babic, R. Tsu, and R.F. Greene, *Phys. Rev. B*, **45**, 14150 (1992).
40. B. Delley and E.F. Steigmeier, *Appl. Phys. Lett.*, **67**, 2370 (1995).
41. Y. Kanemitsu, *J. Lumin.*, **100**, 209 (2002).
42. E. Degoli and S. Ossicini, *Surf. Sci.*, **470**, 32 (2000).
43. Y. Kanemitsu, N. Shimizu, T. Komoda, P.L.F. Hemment, and B.J. Sealy, *Phys. Rev. B*, **54**, 14329 (1996).
44. R. Jenkins and R.L. Snyder, *Introduction to X-Ray Powder Diffractometry*. New York: Wiley (1996).
45. Although Scherrer analaysis is known to be inaccurate for determining the absolute size of nano-scale particles [see, for example, Lee and Stein, J. Phys. Chem, **91**, 2450 (1987)], we believe the trend demonstrated from the Scherrer analysis to be valid.
46. S. Takeoka, M. Fujii, and S. Hayashi, *Phys. Rev. B*, **62**, 16820 (2000).
47. S. Guha, S.B. Qadri, R.G. Musket, M.A. Wall, and T. Shimizu-Iwayama, *J. Appl. Phys.*, **88**, 3954 (2000).
48. S. Schuppler, S.L. Friedman, M.A. Marcus, D.L. Adler, Y.H. Xie, F.M. Ross, Y.J. Chabal, T.D. Harris, L.E. Brus, W.L. Brown, E.E. Chaban, P.F. Szajowski, S.B. Christman, and P.H. Citrin, *Phys. Rev. B*, **52**, 4910 (1995).
49. G. Franzo, F. Iacona, C. Spinella, S. Cammarata, and M.G. Grimaldi, *Mater. Sci. Eng., B*, **69**, 454 (2000).
50. E. Borsella, S. Botti, M. Cremona, S. Martelli, R.M. Montereali, and A. Nesterenko, *J. Mater. Sci. Lett.*, **16**, 221 (1997).
51. F. Koch and V. Petrova, *J. Non-Cryst. Solids*, **198**, 840 (1996).
52. P. Mishra and K.P. Jain, *Mater. Sci. Eng., B*, **95**, 202 (2002).
53. L.N. Dinh, L.L. Chase, M. Balooch, W.J. Siekhaus, and F. Wooten, *Phys. Rev. B*, **54**, 5029 (1996).
54. L. Nikolova, R.G. Saint-Jacques, C. Dahmoune, and G.G. Ross, *Surf. Coat. Technol.*, **203**, 2501 (2009).
55. V. Levitcharsky, R.G. Saint-Jacques, Y.Q. Wang, L. Nikolova, R. Smirani, and G.G. Ross, *Surf. Coat. Technol.*, **201**, 8547 (2007).
56. L. Nikolova, R.G. Saint-Jacques and G.G. Ross, *Ultramicroscopy*, **110**, 144 (2010).
57. Y.Q. Wang, T. Li, W.S. Liang, X.F. Duan, and G.G. Ross, *Nanotechnology*, **20**, art. no. 315704 (2009).
58. J. Valenta, N. Lalic, and J. Linnros, *Appl. Phys. Lett.*, **84**, 1459 (2004).
59. L. Ding, T.P. Chen, Y. Liu, M. Yang, J.I. Wong, K.Y. Liu, F.R. Zhu, and S. Fung, *Nanotechnology*, **18**, 6 (2007).

Downloaded 13 Sep 2010 to 137.122.27.231. Redistribution subject to ECS license or copyright; see http://www.ecsdl.org/terms_use.jsp

60. A. Lacombe, B. Kadari, F. Beaudoin, D. Barba, F. Martin, and G.G. Ross, *Nanotechnology*, **19**, 6 (2008).
61. L.E. Ramos, J. Furthmuller, and F. Bechstedt, *Phys. Rev. B*, **71**, 7 (2005).
62. E. Neufeld, S. Wang, R. Apetz, C. Buchal, R. Carius, C.W. White, and D.K. Thomas, *Thin Solid Films*, **294**, 238 (1997).
63. K. Sato and K. Hirakuri, *J. Appl. Phys.*, **97**, 5 (2005).
64. M.V. Stepikhova, L.V. Krasil'nikova, Z.F. Krasil'nik, V.G. Shengurov, V.Y. Chalkov, S.P. Svetlov, D.M. Zhigunov, V.Y. Timoshenko, and P.K. Kashkarov, *J. Cryst. Growth*, **288**, 65 (2006).
65. D. Pacifici, A. Irrera, G. Franzo, M. Miritello, F. Iacona, and F. Priolo, *Physica E*, **16**, 331 (2003).
66. V.A. Dan'ko, I.Z. Indutnyi, V.S. Lysenko, I.Y. Maidanchuk, V.I. Min'ko, A.N. Nazarov, A.S. Tkachenko, and P.E. Shepelyavyi, *Semiconductors*, **39**, 1197 (2005).
67. J.C. Aubry, T. Tyliszczak, A.P. Hitchcock, J.M. Baribeau, and T.E. Jackman, *Phys. Rev. B*, **59**, 12872 (1999).
68. H. Domer and O. Bostanjoglo, *Rev. Sci. Instrum.*, **74**, 4369 (2003).
69. B.J. Siwick, J.R. Dwyer, R.E. Jordan, and R.J.D. Miller, *Science*, **302**, 1382 (2003).
70. W.E. King, G.H. Campbell, A. Frank, B. Reed, J.F. Schmerge, B.J. Siwick, B.C. Stuart, and P.M. Weber, *J. Appl. Phys.*, **97**, 27 (2005).
71. J.M. Thomas, , *Angewandte Chemie-International Edition*, **44**, 5563 (2005).
72. T. LaGrange, M.R. Armstrong, K. Boyden, C.G. Brown, G.H. Campbell, J.D. Colvin, W.J. DeHope, A.M. Frank, D.J. Gibson, F.V. Hartemann, J.S. Kim, W.E. King, B.J. Pyke, B.W. Reed, M.D. Shirk, R.M. Shuttlesworth, B.C. Stuart, B.R. Torralva, and N.D. Browning, *Appl. Phys. Lett.*, **89**, 3 (2006).
73. B.W. Reed, M.R. Armstrong, N.D. Browning, G.H. Campbell, J.E. Evans, T. LaGrange, and D.J. Masiel, *Microsc. Microanal.*, **15**, 272 (2009).
74. C.V. Cojocaru, C. Harnagea, A. Pignolet, and F. Rosei, *IEEE Trans. Nanotechnol.*, **5**, 470 (2006).
75. C.V. Cojocaru, C. Harnagea, F. Rosei, A. Pignolet, M.A.F. van den Boogaart, and J. Brugger, *Appl. Phys. Lett.*, **86**, 183107 (2005).
76. C.V. Cojocaru, F. Ratto, C. Harnagea, A. Pignolet, and F. Rosei, *Microelectron. Eng.*, **80**, 448 (2005).
77. C. Harnagea, C.V. Cojocaru, R. Nechache, O. Gautreau, F. Rosei, and A. Pignolet, *Int. J. Nanotechnol.*, **5**, 930 (2008).
78. C.V. Cojocaru, A. Bernardi, J.S. Reparaz, M.I. Alonso, J.M. MacLeod, C. Harnagea, and F. Rosei, *Appl. Phys. Lett.*, **91**, 113112 (2007).
79. F. Ratto, F. Rosei, A. Locatelli, S. Cherifi, S. Fontana, S. Heun, P.D. Szkutnik, A. Sgarlata, M. De Crescenzi, and N. Motta, *Appl. Phys. Lett.*, **84**, 4526 (2004).
80. F. Ratto, S. Heun, O. Moutanabbir, and F. Rosei, *Nanotechnology*, **19**, 265703 (2008).
81. F. Ratto, A. Locatelli, S. Fontana, S. Kharrazi, S. Ashtaputre, S.K. Kulkarni, S. Heun, and F. Rosei, *Small*, **2**, 401 (2006).
82. F. Ratto, F. Rosei, A. Locatelli, S. Cherifi, S. Fontana, S. Heun, P.D. Szkutnik, A. Sgarlata, M. De Crescenzi, and N. Motta, *J. Appl. Phys.*, **97**, 043516 (2005).

Downloaded 13 Sep 2010 to 137.122.27.231. Redistribution subject to ECS license or copyright; see http://www.ecsdl.org/terms_use.jsp